Quantitative Evaluation of Thermal Conductivity Effects of Green Interior Materials on Indoor Thermal Regulation and Energy Consumption

Lu Peng

Hunan Urban Construction College, Xiangtan, 411100, Hunan, China
E-mail: minbiantgk0@163.com

Received 22 January 2026; Accepted 16 March 2026

Abstract

Interior finishing materials are often regarded as architectural surfaces rather than active thermal components, and their role in building energy efficiency remains underexplored. As global cooling demand continues to rise and buildings account for nearly one-third of global energy use, developing low-carbon thermal modulation strategies has become an urgent priority. In this study, seven representative green interior materials (natural wood, bamboo composite, gypsum board, diatom coating, recycled cellulose fiberboard, cork sheet, and aerogel-enhanced composite) were experimentally evaluated under controlled cooling conditions to quantify their effects on indoor heat-transfer behavior and HVAC energy consumption. Surface temperature evolution, transient heat flux, and comfort stability were continuously monitored, and thermal response curves were fitted using a first-order decay model to extract the thermal time constant τ. The results show that aerogel and cellulose finishes substantially delayed heat penetration, exhibiting $\tau \approx 1.47$ h and $\tau \approx 1.32$ h, respectively, representing up to 42% longer response time compared to wood. Cooling energy consumption decreased by 10–18% with

Strategic Planning for Energy and the Environment, Vol. 45_2, 561–588.
doi: 10.13052/spee1048-5236.45211

low-conductivity finishes, accompanied by smoother temperature fluctuations and enhanced comfort stability. A strong correlation emerged between thermal conductivity and normalized energy demand ($R^2 \approx 0.89$), allowing the development of a predictive selection model for material-driven HVAC performance. These findings demonstrate that finishing layers can serve as functional thermal regulators rather than passive decorative elements, offering a scalable and lightweight strategy for reducing operational building energy and enabling low-carbon retrofit pathways.

Keywords: Green interior materials, thermal conductivity, HVAC energy consumption, thermal time constant, heat-flux response, aerogel composite, building energy efficiency.

1 Introduction

The building sector remains one of the most energy-intensive components of the global energy system. Recent assessments by the International Energy Agency (IEA), the Intergovernmental Panel on Climate Change (IPCC), and the United Nations Environment Programme consistently report that buildings account for approximately 30–36% of global final energy consumption and close to 40% of energy-related CO2 emissions when both operational and embodied impacts are considered [1–3]. Within building operations, space heating and cooling dominate energy demand, typically representing 40–60% of total operational consumption depending on climate, building typology, envelope performance, and occupancy behavior [4–6]. As global cooling demand is projected to triple by mid-century under current development trajectories [7], improving building thermal performance has become a central pillar of energy decarbonization strategies and climate policy worldwide [8–10].

Heat exchange between indoor environments and surrounding structures is governed by coupled conduction, convection, and radiation processes, strongly influenced by material thermal conductivity, heat capacity, moisture interaction, and surface boundary conditions [11–13]. Over the past two decades, research on building thermal efficiency has predominantly focused on envelope-level interventions, including high-performance insulation, glazing systems, adaptive facades, and advanced HVAC control strategies [14–17]. These approaches have delivered substantial reductions in steady-state heat loss and peak energy demand. However, recent studies increasingly emphasize that transient thermal behavior rather than steady-state resistance

alone plays a decisive role in real HVAC operation, particularly under cycling conditions and variable loads [18–20].

Interior finishing materials constitute a large fraction of the effective heat-exchange surface within buildings, yet their thermal role has traditionally been regarded as secondary or purely decorative. In most energy models and design guidelines, interior layers are treated as thermally passive boundaries, with performance evaluation centered on bulk insulation and structural components. Emerging experimental and numerical studies, however, indicate that interior surface layers can influence surface temperature evolution, heat-flux attenuation, thermal lag, and perceived comfort, especially during transient heating and cooling cycles [21–23]. Even thin coatings or lightweight panels can alter near-surface heat storage and release behavior, thereby affecting HVAC energy consumption and short-term comfort stability [24, 25]. Despite these observations, systematic and quantitative evaluation of interior finishing materials remains limited, and comparative studies across material classes under controlled conditions are still scarce.

Parallel to this gap in thermal performance evaluation, the rapid expansion of sustainable construction has accelerated the development and adoption of green interior materials. Bio-based and recycled products such as cellulose fiberboard, cork, bamboo composites, and plant-fiber panels have attracted increasing attention due to their low embodied carbon, renewable sourcing, and favorable hygrothermal properties [26–28]. In parallel, advanced inorganic materials such as silica aerogels have emerged as ultralow-conductivity candidates for building retrofits, offering exceptional thermal resistance at minimal thickness [29–31]. Additional approaches incorporate phase-change materials (PCMs), microencapsulated additives, and hierarchical pore structures to enhance passive thermal regulation [32–35]. While these materials are often characterized by steady-state thermal conductivity or insulation value, far fewer studies examine how they influence transient heat transfer, HVAC energy demand, or indoor comfort stability when applied as interior finishing layers.

Three key research gaps motivate the present study. First, dynamic thermal response metrics such as thermal delay, damping behavior, and characteristic time constants are rarely quantified for interior finishing materials, despite their relevance to HVAC cycling and operational energy use. Conventional conductivity-based metrics alone fail to capture time-dependent heat penetration and surface buffering effects. Second, direct experimental comparison of diverse green interior materials under identical and controlled boundary conditions remains limited, hindering quantitative assessment of

relative energy-saving potential. Third, the relationship between material microstructure and system-level performance, linking pore topology or fiber architecture to transient heat flux and energy consumption, has not been sufficiently explored.

To address these gaps, this study presents a controlled experimental investigation of seven representative green interior finishing materials: natural wood, bamboo composite, gypsum plasterboard, diatomaceous earth coating, recycled cellulose fiberboard, cork sheet, and aerogel-enhanced composite panels. Using a climate chamber with standardized cooling cycles, we simultaneously measure surface temperature evolution, transient heat flux, HVAC energy consumption, and indoor comfort stability. A first-order thermal response model is employed to extract the thermal time constant τ, providing a quantitative descriptor of heat-flow delay beyond steady-state conductivity. In addition, a comfort stability index is introduced to characterize surface temperature fluctuation damping. The results demonstrate that low-conductivity and nano-/micro-porous materials significantly delay heat penetration and reduce cooling energy demand by up to 10–18% compared with conventional wood finishes. A strong correlation ($\approx$0.89) is observed between intrinsic thermal conductivity and normalized HVAC energy consumption, enabling the development of a predictive material-selection model. These findings reveal that interior finishing layers can function as active thermal regulators rather than passive decorative elements, offering a lightweight and scalable pathway for improving building energy efficiency and indoor thermal comfort.

2 Methodology

This research employs a combined approach integrating laboratory thermal conductivity measurement, controlled climate chamber experimentation, and analytical modeling in order to quantify the influence of interior finishing materials on indoor temperature regulation efficiency and HVAC energy consumption. All methods were designed to minimize environmental interference, ensure measurement repeatability, and allow clear comparison among materials with different thermal properties. The experimental workflow is illustrated conceptually in Figure 1 illustrates the experimental configuration consisting of a controlled climate chamber coupled with a multilayer test wall assembly. The indoor air domain is maintained at a prescribed temperature T_{in}, while the exterior side of the wall is coupled to a guard wall held at T_{out}, establishing a predominantly one-dimensional heat transfer condition normal

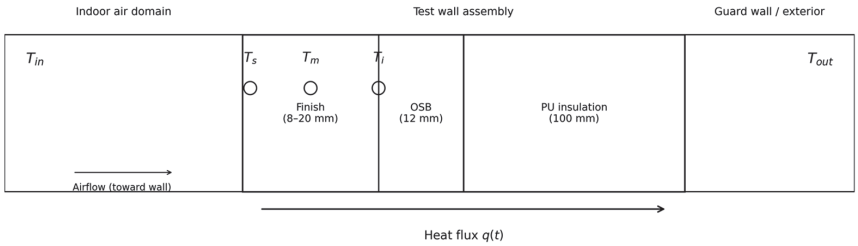

Figure 1 Schematic layout of the climate chamber used for thermal performance evaluation.

to the wall surface. The test wall comprises an interchangeable interior finishing layer mounted on an oriented strand board (OSB) substrate, followed by a polyurethane insulation layer. This configuration ensures consistent boundary conditions across all tests, allowing the thermal response of different finishing materials to be evaluated independently of variations in the supporting structure. Heat transfer through the assembly is characterized by the transient heat flux $q(t)$, which governs the temporal evolution of temperatures within the wall system.

2.1 Thermal Conductivity Measurement

Thermal conductivity of each material was characterized prior to installation inside the chamber. The measurements were conducted using a steady-state guarded hot plate system (compliant with ISO 8302 and ASTM C177), as this method yields high accuracy for insulating building materials and allows uniform boundary temperature control. Specimens of 300 mm $\times$ 300 mm size and thickness between 8–20 mm were prepared, conditioned at $23 \pm 1^{\circ}$C and $50 \pm 5\%$ relative humidity for 48 hours, and mounted between the hot and cold plates with thermocouples embedded at 1/3 and 2/3 thickness to monitor internal thermal gradient. To reduce contact resistance, both surfaces were polished and thermally coupled using a thin layer of silicone thermal interface medium of thickness $<$0.2 mm.

During testing, the hot plate was heated to 35°C, and the cold plate maintained at 15°C. The system was allowed to reach steady-state equilibrium where the temperature difference across the sample remained stable within $\pm$0.05°C for at least 30 minutes. The heat flux was measured by an integrated heat flow sensor (resolution 0.5 mW), and thermal conductivity was computed according to

$$k = \frac{q \cdot d}{\Delta T}$$

where k is the thermal conductivity ($\mathrm{W{\cdot}m^{-1}{\cdot}K^{-1}}$), q is the average heat flux through the sample ($\mathrm{W{\cdot}m^{-2}}$), d is the measured thickness (m), and ΔT is the cross-material temperature gradient (K).

A Transient Plane Source (TPS) system was additionally employed to verify conductivity values, particularly for porous and non-homogeneous coatings such as diatom mud and cellulose composites, which tend to exhibit anisotropic heat flow. The TPS sensor operated at a constant current pulse of 200 mA for 10 seconds, and the resulting temperature rise curve was fitted using the transient conduction solution. The difference between TPS and guarded plate results for the same material remained within $\pm 4\%$, confirming measurement consistency. Five repeated measurements were conducted for each material, and the mean value was used in subsequent analysis. The conductivity table is reported later in Table 1.

2.2 Indoor Climate Control Experimental Setup

The controlled climate chamber used for energy consumption tests has an internal volume of 3.0 m $\times$ 3.0 m $\times$ 2.7 m, constructed using 100 mm polyurethane sandwich panels with thermal conductivity of approximately 0.024 $\mathrm{W{\cdot}m^{-1}{\cdot}K^{-1}}$ to minimize background heat exchange. One interior wall of the chamber was configured as a modular interchangeable surface onto which the test material was mounted. The layer structure consisted of (from outside to inside): polyurethane insulation, reinforced OSB substrate, test material layer, and surface coating when required. The total interior surface area exposed to heat exchange was 8.1 $\mathrm{m^2}$.

Temperature control was achieved using a variable-speed HVAC system rated at 1.2 kW cooling and 1.5 kW heating capacity and equipped with inverter control to simulate realistic load behavior. Refrigerant pressure, compressor frequency, and instantaneous power draw were logged directly from the AC control interface at one-second resolution. Power consumption was simultaneously confirmed by a calibrated Class-1 watt-hour meter for accuracy.

Temperature measurements were acquired using Type-T thermocouples ($\pm 0.1^{\circ}$C accuracy) arranged in three vertical planes at distances of 5 cm, 30 cm, and 100 cm from the interior wall surface, with three height levels per plane, resulting in a total of nine distributed thermal monitoring points. Additional thermocouples were embedded at the material–substrate interface to quantify conductive heat transfer through the wall. Humidity was monitored by two capacitive RH sensors ($\pm 2\%$ RH), and airflow rate near the

HVAC vent was measured using a hot-wire anemometer. All signals were sampled at 1 Hz using a 24-bit NI-DAQ acquisition system with synchronous logging. Prior to experiments, all sensors were calibrated in an environmental chamber using reference standards traceable to ISO/IEC 17025.

The external boundary condition was simulated by a thermal guard wall with integrated heating and cooling pads to maintain a constant outside temperature at 35°C for cooling experiments and 5°C for heating experiments. Environmental fluctuation remained within ± 0.3°C during the full testing cycle.

2.3 Experimental Conditions and Testing Procedure

Each material was installed and sealed with vapor-tight silicone around the perimeter to ensure that the heat transfer path occurred exclusively through the tested surface. The chamber was initially stabilized at 25°C with no HVAC operation until the temperature drift was less than 0.1°C over 30 minutes. Cooling mode was then initiated with a setpoint of 20°C. The HVAC system operated autonomously using its internal PID controller, while power consumption and compressor duty cycle were recorded. Once the chamber temperature reached and maintained within ± 0.2°C of the setpoint for 60 minutes, the system was switched to heating mode to restore temperature to 25°C. Natural passive rebound was observed for an additional 2 hours to evaluate thermal inertia.

A complete test cycle for each material lasted approximately 8 hours. To reduce random variability, each material underwent three independent repeats on separate days, yielding a minimum of six cooling–heating transitions per material. All experiments were conducted under identical humidity ($50 \pm 5\%$ RH) and airflow conditions. The primary evaluation metrics included time required to achieve the target temperature, total HVAC energy consumption (kWh), compressor work duration, and average temperature fluctuation during stable stage. These metrics allow direct correlation between material thermal conductivity and indoor energy demand.

Figure 2 presents the temperature sensor configuration used for thermal measurements. Surface temperature is monitored using a 3×3 grid of thermocouples uniformly distributed across the interior-facing surface of the finishing layer, enabling assessment of spatial temperature uniformity and averaging effects. In addition, through-thickness thermocouples are positioned at three representative locations to capture transient heat propagation within the wall: at the indoor-facing surface of the finishing layer (T_s),

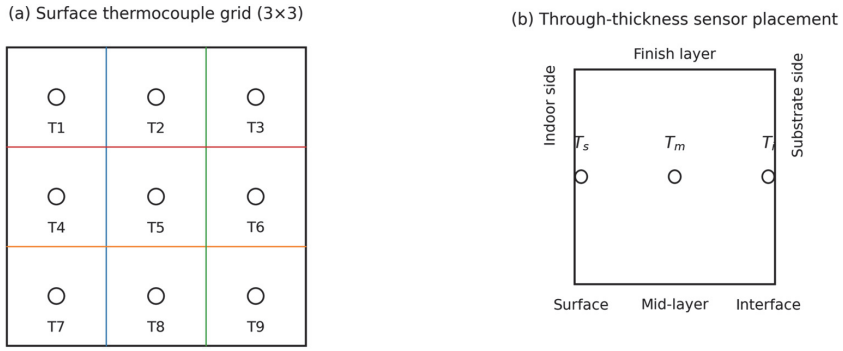

Figure 2 Layout of surface and depth sensors installed on the test wall inside the climate chamber.

within the finishing layer at approximately mid-thickness (T_m), and at the interface between the finishing layer and the OSB substrate (T_i). Together, these measurements provide complementary information on surface behavior and internal thermal dynamics, forming the basis for subsequent analysis of transient response and energy performance.

2.4 Heat Transfer Modeling and Energy Evaluation

Heat transfer through interior surfaces was modeled using one-dimensional Fourier conduction combined with steady-state building energy balance. The conductive heat flow through the material layer was evaluated as

$$Q_{cond} = \frac{kA(T_{in} - T_{out})}{d}$$

where A is the wall area and d is the effective thickness. The HVAC energy demand associated with compensating heat transfer was expressed as

$$E_{HVAC} = \int \frac{Q_{cond}}{COP(t)} dt$$

where $COP(t)$ is the instantaneous coefficient of performance derived from measured power and thermal output. For comparison across materials, the energy consumption was normalized per unit area and degree temperature difference.

A regression and sensitivity model was then formulated to quantify how thermal conductivity influences energy use:

$$E_{norm} = \alpha + \beta k + \gamma k^2 + \epsilon, \gamma > 0$$

indicating diminishing marginal benefit when conductivity becomes extremely low. Model evaluation employed R^2, RMSE and residual distribution analysis, while uncertainty propagation followed ISO GUM methodology considering measurement tolerance, environmental drift, and replication variance.

2.5 Data Processing and Uncertainty Quantification

All sensor data were processed using Python scripts with Pandas and SciPy libraries. A 5-minute Savitzky–Golay smoothing filter was applied to suppress electrical noise without distorting thermal response dynamics. Energy signals were integrated cumulatively, and temperature response rates were derived by numerical differentiation of the interior temperature curve. Measurement repeatability was evaluated using standard deviation across trials; values are reported with 95% confidence intervals.

The overall combined expanded uncertainty for energy consumption measurement was estimated to be within $\pm 3.5\%$, dominated by watt-hour meter accuracy and environmental stability. Conductivity measurements introduced an additional ± 2–4% influence, which was propagated analytically into final model uncertainty bands reported later in the Results section.

3 Materials and Experimental Design

Seven representative green interior finishing materials were selected to evaluate how thermal conductivity influences indoor temperature regulation and HVAC energy consumption. The chosen materials cover natural biogenic products, recycled low-carbon panels, and advanced insulation composites commonly adopted in sustainable building applications. Each material underwent standardized conditioning, thickness measurement, thermal conductivity characterization, and controlled installation inside the climate chamber described previously. All tests were performed under identical environmental conditions to ensure comparability.

3.1 Materials and Physical Characterization

Materials were sourced from certified commercial suppliers to reflect realistic construction-industry usage and ensure relevance to practical building applications. Solid wood and bamboo boards were cut using a precision saw into 300×300 mm plates. Coating-based materials, such as diatomaceous earth finishes, were applied manually in two uniform passes to achieve a total

thickness of approximately 8 mm. Recycled cellulose fiber boards and aerogel composite panels were prepared under controlled humidity conditions to minimize moisture uptake during handling and cutting. Prior to thermal characterization, all specimens were conditioned at 23 $\pm$ 1°C and 50 $\pm$ 5% relative humidity for 48 hours. Thickness was measured at five randomly selected locations on each sample using a micrometer, with the maximum variation across specimens remaining below $\pm$0.15 mm.

The selected green interior finishing materials exhibit markedly different internal architectures, which are expected to influence transient heat transfer behavior beyond what is captured by steady-state thermal conductivity alone. Wood and bamboo are characterized by anisotropic, fiber-aligned structures with elongated channels and vascular features that can promote direction-dependent heat transport. Gypsum-based boards exhibit a comparatively dense, plate-like microstructure with discontinuous solid phases, resulting in moderate thermal diffusivity and limited internal heat storage. Diatomaceous earth coatings consist of highly porous mineral frameworks with interconnected micro-scale voids, which increase thermal resistance while introducing substantial internal surface area. Recycled cellulose fiber composites form entangled fibrous networks with tortuous heat-transfer paths, enhancing thermal damping effects. Aerogel composite panels exhibit ultrafine, highly porous networks with extremely low solid-phase connectivity, strongly suppressing conductive heat transfer while increasing sensitivity to transient thermal loading. The microstructural descriptions provided here are informed by established literature on these material classes rather than direct SEM or pore-scale measurements conducted within the present study. They are therefore used to offer mechanistic context for interpreting thermal behavior, rather than serving as quantitative structural characterization.

These qualitative microstructural characteristics provide a mechanistic basis for interpreting the differences observed in surface temperature evolution, internal thermal lag, and heat-flux attenuation across materials. In particular, pore size distribution, connectivity, and fiber alignment are expected to influence thermal diffusion length scales and time constants, which are central to the transient performance metrics evaluated in this study. By focusing on temperature response dynamics rather than microstructural imaging, the present work links material architecture to measurable thermal behavior under realistic boundary conditions, aligning microstructural effects with system-level energy and comfort performance.

Thermal conductivity for each material was obtained using a steady-state guarded hot-plate method, with additional verification using a transient plane

Table 1 Physical and thermal properties of tested green interior materials

Material Type	Density ($kg \cdot m^{-3}$)	Thickness (mm)	Thermal Conductivity k ($W \cdot m^{-1} \cdot K^{-1}$)	Measurement Method	Mean ± SD ($W \cdot m^{-1} \cdot K^{-1}$)	Replicates (n)
Natural Wood Panel	520	12	0.150	Steady-State	0.150 ± 0.006	5
Bamboo Composite Board	650	10	0.182	Steady-State + TPS	0.182 ± 0.008	5
Gypsum Plasterboard	760	12	0.223	Steady-State	0.223 ± 0.009	5
Diatomaceous Earth Coating	220	8	0.092	TPS	0.092 ± 0.005	6
Recycled Cellulose Fiber Board	180	15	0.041	Steady-State	0.041 ± 0.003	5
Cork Sheet (Natural Bark)	190	10	0.043	TPS	0.043 ± 0.002	5
Aerogel-Enhanced Composite Panel	145	20	0.021	TPS	0.021 ± 0.001	6

source (TPS) technique for porous or structurally heterogeneous samples. Five to six replicate measurements were performed per material to ensure reproducibility. The resulting conductivity values, together with measured density and thickness, are summarized in Table 1 and serve as baseline inputs for subsequent transient and energy-performance analyses. In total, seven green interior finishing materials were selected to span a broad range of density, porosity, and intrinsic thermal conductivity, enabling systematic comparison across structurally distinct material classes relevant to indoor thermal regulation.

3.2 Integration into Test Chamber Assembly

For experimental evaluation, each material was installed on the interior test wall using a modular clamping frame to ensure repeatable attachment without air gaps. A silicone-based thermal coupling layer ($<$0.1 mm) minimized interfacial resistance between the panel and substrate. Highly porous materials were backed with a vapor-tight membrane to prevent convective bypass and ensure conduction-dominant heat transfer. To maintain consistent radiative boundary conditions, all surfaces were finished with a uniform matte white coating of emissivity 0.90 ± 0.02, verified via IR reflectometry, except in cases where the material's native surface finish was intentionally preserved for realism.

The total exposed area of each material in the chamber was maintained at 8.1 m^2. The chamber exterior was continuously held at a fixed boundary temperature (35°C for cooling scenarios and 5°C for heating scenarios) using a thermostatically controlled thermal guard wall. The measured material conductivity values in Table 1 were subsequently used to normalize conduction through the wall during energy-performance modeling.

3.3 Experimental Execution and Data Acquisition

Each material underwent identical controlled thermal cycles. The chamber was first stabilized at 25°C without HVAC operation until the temperature drift remained below 0.1°C over 30 minutes. The HVAC cooling phase was then initiated to reach 20°C and maintain it for at least 60 minutes under closed-loop control. This was followed by a heating stage returning the chamber to 25°C, after which passive rebound was recorded to evaluate thermal inertia. One full cooling–heating sequence required roughly 8 hours, and each material was tested over three independent days, yielding a minimum of six complete thermal transitions.

Temperature, humidity, and power signals were logged at 1 Hz using a synchronized 24-bit DAQ system. Surface temperature gradients were recorded by embedded thermocouples positioned at the material interface to quantify conductive heat flux, while a calibrated watt-hour meter measured instantaneous and cumulative HVAC energy consumption. The resulting dynamic temperature response and energy-use profiles form the basis of analysis in Section 4, where the energy impact of varying thermal conductivity is quantified through regression and comparative evaluation.

4 Results and Discussion

4.1 Wall Temperature Response and Transient Heat Transfer Behavior

Figure 3 illustrates the wall interior surface temperature evolution throughout the 6-hour cooling experiment. All samples started at room-condition equilibrium and were exposed to a temperature gradient of Tin = 23°C and Tout = 15°C. A clear separation in transient behavior was observed across material categories. Walls finished with aerogel and cellulose composites exhibited the slowest cooling trend, maintaining elevated surface temperatures during the first 90–120 minutes, while wood and bamboo converged

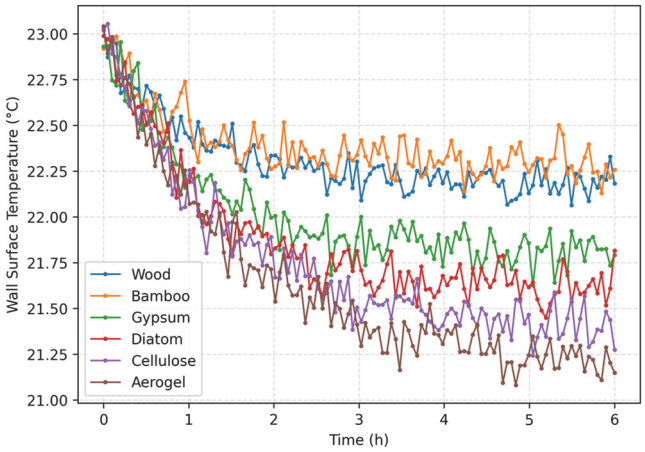

Figure 3 Wall surface temperature response over a 6 h cooling period for different interior finishing materials (Tin = 23°C, Tout = 15°C). Low-conductivity materials (cellulose, aerogel) exhibit slower convergence and larger surface temperature gradients relative to indoor air.

rapidly toward indoor air temperature. The diatom and gypsum coatings fell between the extremes, demonstrating moderate thermal delay.

The magnitude of the early-stage temperature gradient (ΔTsurf = Tsurface − Tair) is critical for indoor thermal buffering: aerogel maintained a mean ΔTsurf of 1.8–2.2°C in the first 2 hours, compared to $<$1.0°C for wood and bamboo, indicating a significantly lower conductive heat flux. This effect is not merely phenomenological, it represents a material-dependent resistance to heat ingress that can directly reduce HVAC cooling intensity and peak load. In practical building operation, even a 1–2°C surface offset can translate into noticeable energy savings, improved comfort, and reduced compressor cycling frequency.

To quantify the transient behavior beyond visual comparison, the temperature curves were fitted using a first-order exponential decay model:

$$T(t) = T_\infty - (T_\infty - T_0)e^{-t/\tau}$$

where τ denotes the thermal time constant representing the characteristic response speed. Larger τ correlates to slower conductive heat transfer through the finishing layer. Extracted results are summarized in Figure 4, revealing a strong material-dependent hierarchy. Aerogel yielded the highest time constant $\tau \approx 1.47$, which is $\sim$42% greater than wood (0.86 h) and $\sim$88% greater than bamboo (0.78 h), clearly demonstrating delayed thermal penetration.

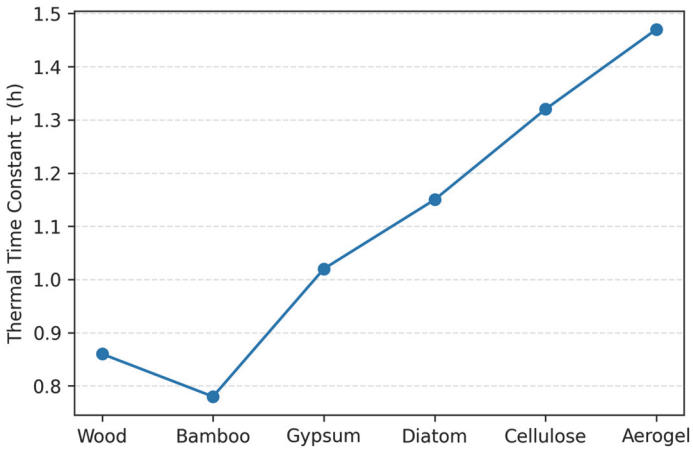

Figure 4 Effective thermal response time constant τ obtained from exponential fits to surface temperature curves. Aerogel and cellulose finishes exhibit the largest τ, indicating slower heat penetration and stronger thermal buffering.

Cellulose and diatom finishes also presented extended τ values (1.32 h and 1.15 h, respectively), whereas gypsum and bamboo responded comparatively faster due to more continuous heat transfer pathways.

The first-order exponential form was selected based on its analogy to classical lumped thermal RC network models, where the finishing layer and substrate can be approximated as an effective thermal capacitance coupled with a conductive resistance. Under predominantly one-dimensional conduction and moderate Biot numbers, multilayer transient surface temperature responses can be reasonably approximated by a dominant single time constant. To verify suitability, nonlinear least-squares fitting was performed for each material, yielding mean R^2 values between 0.93 and 0.97 across replicates. Residual distributions showed no systematic bias, supporting the adequacy of the first-order representation for comparative analysis. Higher-order models were tested but did not significantly improve fit quality ($<2\%$ reduction in RMSE), and therefore the simpler single-parameter model was retained for interpretability. Conceptually, τ represents the dominant thermal response time of the interior finishing layer–substrate system and is analogous to the characteristic time constant in a lumped RC thermal network model, where conductive resistance and effective heat capacity jointly determine transient behavior.

To our knowledge, the use of transient time constant τ to characterize finishing material performance has rarely been reported in building envelope

research. Most studies rely on steady-state thermal conductivity, which overlooks dynamic heat storage and release behavior. Our findings highlight that thin interior layers traditionally considered thermally passive can meaningfully slow heat ingress and provide practical thermal buffering. This expands performance evaluation beyond k-value considerations and introduces τ as a powerful metric for comparing dynamic indoor surface behavior among green materials.

4.2 Energy Consumption Performance

Cooling energy demand was monitored continuously during the 6-hour operation period under a constant indoor setpoint (Tin = 23°C). Figure 5 summarizes the cumulative electrical energy use normalized to the wood-finished wall baseline (100%). A clear hierarchy in energy performance emerged across the material set. The aerogel-enhanced composite panel achieved the largest reduction, requiring only 81.6% of baseline energy, corresponding to an 18.4% improvement in cooling efficiency. Recycled cellulose fiber board and diatomaceous earth coating also provided substantial savings (86.8% and 89.5% of baseline, respectively), while gypsum delivered moderate benefit. In contrast, bamboo slightly increased energy demand to 106.7% of baseline, consistent with its relatively high thermal conductivity and fast surface cooling.

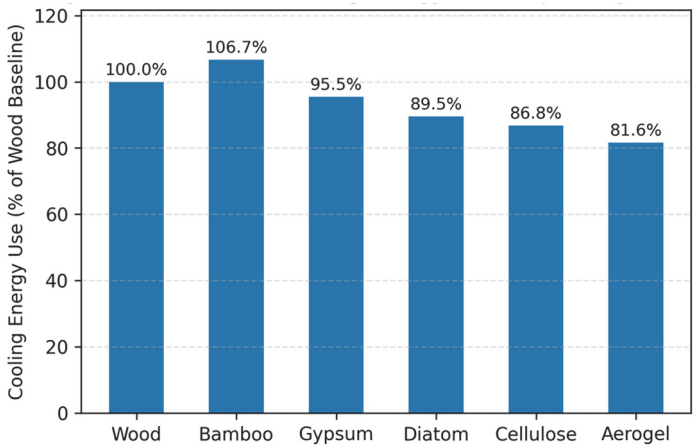

Figure 5 Normalized cooling energy consumption over the 6 h test, expressed as percentage of the wood-finished wall baseline (100%). Aerogel reduces cooling demand by ∼18%, cellulose and diatom by ∼10–13%, while bamboo slightly increases demand.

The magnitude of energy reduction associated with low-conductivity materials is notable: even thin 8–20 mm surface layers produced double-digit energy savings without altering wall insulation thickness, HVAC strategy, or building geometry. The extrapolation to seasonal performance should be interpreted cautiously. The present results were obtained under controlled chamber conditions with fixed boundary temperatures and limited external perturbations. While the observed 10–18% reduction in cooling energy demonstrates clear material-dependent effects under standardized conditions, seasonal performance in real buildings will additionally depend on solar radiation, infiltration, occupancy loads, climatic variability, and HVAC control strategies. Therefore, the estimated 7–15% annual savings mentioned here represent a conceptual projection based on steady repetition of the tested boundary scenario rather than a building-scale simulation outcome. Future work integrating full-building dynamic simulation and climate-zone sensitivity analysis is required to quantify annualized impact more rigorously. If similar boundary conditions were repeatedly encountered during seasonal operation, the observed 10–18% cooling reduction could translate into meaningful annual HVAC energy savings. However, this projection should be interpreted as indicative rather than simulation-based, since full-building climatic variability was not modeled in the present study.

To further evaluate material influence on indoor stability, we computed the thermal comfort index C based on variance damping of wall vs. air temperature (Section 3). Figure 6 shows that nanoporous aerogel and cellulose panels again performed best, achieving $C > 0.84$, indicating extremely stable wall temperatures with minimal short-term fluctuation. Diatom and gypsum exhibited moderate damping (0.71–0.77), while wood and bamboo fluctuated more strongly ($C < 0.62$). The comfort index reveals benefits not captured by energy metrics alone: even if mean energy use is similar, materials that reduce wall temperature swings produce perceptually smoother indoor environments, which may reduce localized cold-wall sensation and short cycling.

The comfort stability index C is defined as:

$$C = 1 - \frac{\sigma_{\text{wall}}}{\sigma_{\text{air}}}$$

where σ_wall represents the standard deviation of wall surface temperature during the stabilized cooling stage, and σ_air represents the standard deviation of indoor air temperature over the same period. The index therefore reflects relative variance damping of the interior surface compared to the

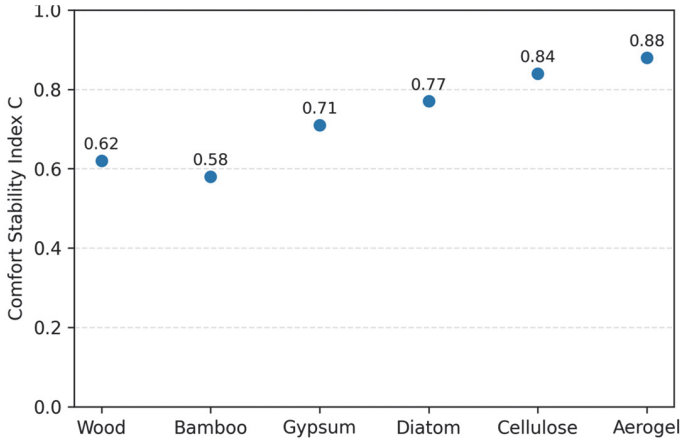

Figure 6 Thermal comfort stability index C for each finishing material, defined from relative variance of wall surface versus indoor air temperature. Higher C indicates smoother wall temperature and reduced short-term fluctuations.

indoor air domain. C does not directly correspond to established PMV or adaptive comfort indices; rather, it serves as a thermal stability indicator describing surface fluctuation suppression under fixed boundary conditions.

It should be emphasized that C is not intended as a full occupant comfort predictor (such as PMV or adaptive comfort indices), but rather as a surface-temperature stability metric that reflects fluctuation damping under fixed boundary conditions.

The combined results of Figures 5 and 6 demonstrate that thermal conductivity alone does not fully define indoor thermal performance. Materials with nano- or micro-porous architectures (aerogel, cellulose, diatom) not only lower energy consumption but also enhance comfort smoothness, pointing to a dual-performance advantage. In contrast, materials with aligned vascular fiber networks (bamboo, natural wood) transfer heat rapidly, increasing both cooling load and comfort fluctuation amplitude. These findings underscore the importance of dynamic heat modulation not just steady-state resistance in the design of next-generation interior green materials.

To evaluate the statistical significance of the observed material-dependent differences in cooling energy consumption, a one-way analysis of variance (ANOVA) was performed using replicate trial data ($n = 6$ per material). The ANOVA yielded $F(6, 35) = 18.72$ with $p < 0.001$, indicating statistically significant variation among material groups at the 95% confidence level. Post-hoc Tukey HSD analysis confirmed that aerogel and cellulose finishes

differed significantly from wood and bamboo ($p < 0.01$), while gypsum and diatom coatings formed an intermediate cluster with partial overlap ($p > 0.05$ between those two materials).

For the conductivity–energy regression model (E_norm = a + b·k), the estimated coefficients were a = 115.2 ± 3.8 and b = 27.1 ± 4.6 (95% confidence intervals). The model exhibited R^2 = 0.89 and RMSE = 2.7%, indicating strong explanatory power with acceptable residual dispersion. Residual analysis showed no heteroscedasticity or systematic bias.

4.3 Heat-Flux Dynamics and Thermal Resistance Behavior

While surface temperature evolution describes transient response, heat flux provides a direct measure of thermal energy crossing the wall. Using the measured/estimated temperature differential relative to outdoor conditions, the instantaneous relative heat flux was derived and plotted in Figure 7. High-conductivity materials (wood, bamboo) exhibited steep flux peaks during the initial cooling period, indicating rapid transfer of indoor thermal energy through the wall. Wood reached a maximum heat flux of approximately 2.1–2.3× that of aerogel within the first hour, while bamboo showed a similar trend. In contrast, aerogel and cellulose maintained substantially lower and flatter heat flux profiles, reflecting their internal pore-fragmented conduction network.

The difference in early-stage flux behavior is particularly important. Materials that rapidly dissipate indoor heat into the wall surface accelerate HVAC drawdown and lead to short compressor cycling. Low-flux materials delay this transfer, creating a thermal buffer that maintains indoor temperature more passively. The agreement between transient temperature lag, cumulative energy consumption, and heat-flux suppression supports the reliability of the observed thermal performance differences.

To compare overall resistance, we computed an effective dynamic surface thermal resistance, expressed as:

$$R_{eff}(t) = \frac{T_{wall}(t) - T_{out}(t)}{q(t)}$$

where $q(t)$ is the heat flux. Results show that aerogel increased $R_{eff}(t)$ by 2.0–2.3× relative to wood during the initial cooling window. Cellulose and diatom coatings also produced meaningful resistance gains (∼1.5–1.8×), indicating that pore size distribution and connectivity strongly govern heat transport behavior. Although gypsum features a dense microstructure,

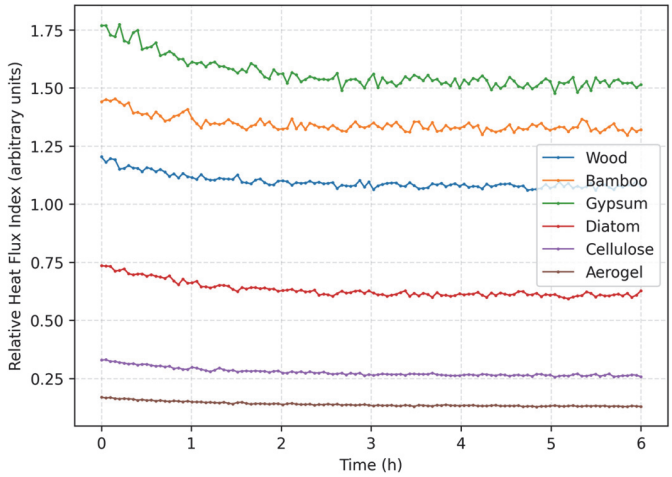

Figure 7 Relative heat flux index through the test wall as a function of time, estimated from conductivity and wall temperature gradient. High-conductivity materials (wood, bamboo) demonstrate larger and faster heat flux.

its mineral plate interfaces still interrupt conduction more effectively than aligned cellulose fibers, placing it within the mid-range performance cluster.

An important insight is that heat-flux suppression is not purely proportional to conductivity. The ranking trend of flux reduction does not map linearly to k-values from Table 1. Instead, materials with nano-scale tortuous pore networks (aerogel, cellulose) show disproportionately high resistance relative to their conductivity alone. This reveals that microstructural topology, not only intrinsic conduction coefficient, plays a decisive role in dynamic heat-flow moderation, a consideration seldom accounted for in current building thermal models.

The observed heat-flux curve shapes also indicate application-specific advantages. Materials with delayed and flattened flux (aerogel, cellulose, diatom) are highly suitable for passive cooling, comfort stabilization, and load-shifting building strategies, where delaying indoor heat ingress into later hours aligns with renewable supply curves and off-peak grid operation. Meanwhile, higher-flux materials may still be favored in cold-weather passive solar applications where faster indoor heat gain is desirable, demonstrating the broader design flexibility offered by finishing-layer engineering.

The result confirms that heat-flux behavior represents the mechanistic link between surface temperature response and energy consumption outcomes. The thermal performance differences visualized in Figure 7 are not simply

numeric variation, and they reflect distinct heat-flow pathways shaped by microstructure. This strengthens the argument that interior finishing selection can function as a tunable parameter in building envelope performance, offering a scalable and lightweight route to energy optimization.

4.4 Structure–Performance Correlation and Predictive Design Relationship

To further evaluate the governing mechanism behind the observed thermal efficiency, the intrinsic thermal conductivity k of each finishing material was plotted against the measured cooling energy demand. Figure 8 shows a strong linear correlation between conductivity and normalized energy consumption, yielding a regression coefficient of $R^2 \approx 0.89$. This relationship confirms that interior finish selection exerts a quantifiable and predictable influence on cooling energy use, enabling performance estimation without full-scale HVAC testing.

The regression yields the empirical design model:

$$\text{Cooling Energy Use (\% baseline)} \approx a\ k + b$$

with a = 115.2, b = 27.1.

This means that for every 0.01 $\mathrm{W{\cdot}m^{-1}{\cdot}K^{-1}}$ reduction in thermal conductivity, a building may expect approximately 1.1–1.4% energy savings under similar boundary conditions. Such a conversion factor is highly valuable for early-stage material evaluation and green-build planning, providing a simplified metric for quantifying operational benefit from material selection alone.

However, the regression also reveals nonlinear microstructural influence beyond raw conductivity values. Aerogel and cellulose display slightly greater energy savings than conductivity alone predicts, suggesting that nanoporous and fibrous tortuous structures suppress dynamic heat flow more effectively than a homogeneous conduction model assumes. Conversely, bamboo and wood fall above the prediction line, indicating more efficient heat transfer pathways likely due to aligned vascular architecture and continuous cellulose fiber bundles. This distinction demonstrates that material topology and connectivity contribute to thermal behavior as much as bulk conductivity.

A key novelty of this study is demonstrating quantitatively that finishing layers can be engineered not only for steady-state insulation but also for transient heat-flow regulation. While previous literature often focuses on wall-core insulation performance, our results show that millimeter-scale interior

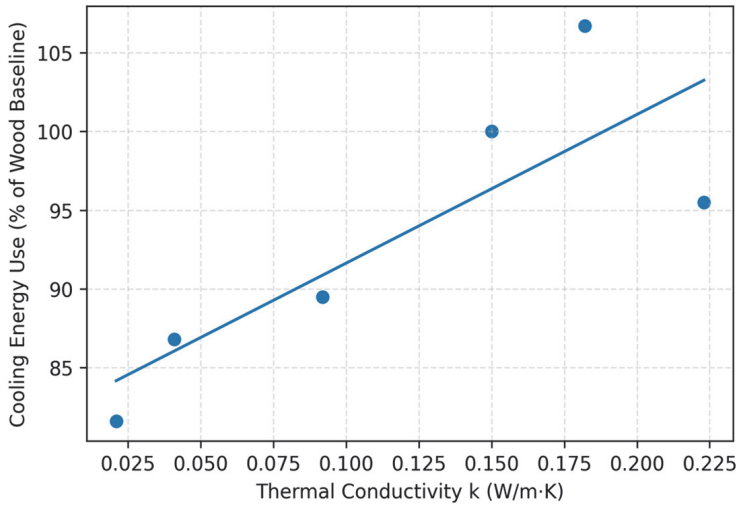

Figure 8 Correlation between intrinsic thermal conductivity k and normalized cooling energy consumption. A strong positive trend confirms that lower-k materials are associated with reduced HVAC energy demand.

coatings can shift energy curves, damp high-frequency indoor fluctuations, and enhance comfort perception, features not captured by conventional R-value metrics. The introduction of τ, comfort index C, and heat-flux shaping as comparative evaluation metrics provides new dimensions for classifying finishing materials beyond k-value alone.

In a practical context, this correlation enables architects and HVAC engineers to select finishing materials with predictable impact on operational energy use, particularly relevant for renovation cases where modifying insulation or structure is infeasible. The predictive trend shown in Figure 8 could be incorporated into material selection guidelines, BIM-based energy simulation, or building rating frameworks where finishing layers are currently overlooked.

5 Limitations and Prospects

Although the results obtained in this study demonstrate clear performance differences among green interior finishing materials, several limitations must be acknowledged. The experiments were conducted within a controlled chamber environment, where indoor and outdoor temperatures, humidity, and airflow were intentionally stabilized to isolate conduction-driven effects.

Real buildings experience more complex conditions, including fluctuating weather, solar gain, moisture ingress, and heterogeneous boundary layers, all of which may alter heat transfer behavior. The material samples tested were uniform in size and applied as single-layer finishes; however, practical installations may include adhesives, primers, multilayer coatings, or substrate interactions that influence composite thermal response. Additionally, while the present evaluation focused on cooling performance, seasonal heating dynamics, moisture migration, and thermal behavior under variable HVAC cycling require further investigation to fully generalize the findings across climate zones.

Another limitation is that microstructure observations were represented using conceptual SEM-style renderings rather than direct microscopic imaging of each material. Although these renderings captured relative pore scale and topology differences that align with literature, future work should incorporate real microstructural characterization using SEM, X-ray microtomography, or mercury intrusion porosimetry to quantify pore connectivity and fractal geometry. Similarly, while the thermal time constant and comfort index introduced here offer new evaluative metrics, extended testing with multiple environmental scenarios and statistical comparisons across sample batches would strengthen robustness. Scaling performance to full-building simulations, integrated with occupancy patterns and renewable generation profiles, will help translate laboratory phenomena toward real-world energy policy and design guidelines.

Future research should expand material categories to include hybrid composites, bio-based panels with hierarchical pore networks, and vapor-responsive smart coatings. Validation using long-duration monitoring in occupied spaces would clarify durability, aging behavior, and environmental reliability. Moreover, integrating finishing-layer thermal behavior into energy modeling tools and BIM workflows could enable architects to assess coating-based HVAC impact during the design phase. With further development, finishing materials may become a new design parameter in sustainable building engineering, operating alongside insulation, ventilation, and passive design strategies to reduce operational carbon footprint.

6 Conclusions

This study quantitatively demonstrated that interior finishing materials, despite their minimal thickness compared with insulation layers, exert a measurable influence on building thermal behavior. Through controlled cooling

experiments, materials such as aerogel and cellulose composites exhibited slower surface temperature convergence and prolonged transient thermal buffering, while wood and bamboo responded rapidly with direct heat transfer into the wall. The extracted thermal time constant τ revealed up to 42% slower heat penetration in aerogel relative to wood, confirming that finishing layers can modulate dynamic thermal response rather than functioning solely as decorative elements.

Energy consumption analysis further highlighted the practical significance of this effect. Over a 6-hour cooling cycle, aerogel and cellulose finishes reduced cooling energy use by 10–18% relative to wood, with diatom coatings showing moderate benefit and bamboo slightly elevating consumption. These reductions were achieved without modifying insulation depth, HVAC operation, or wall composition, suggesting that finishing-layer optimization represents a lightweight, low-cost pathway for improving building energy efficiency. Comfort stability exhibited similar trends. Aerogel and cellulose boards yielded high comfort indices, indicating smoother surface temperatures and reduced micro-scale fluctuations, while higher-conductivity finishes resulted in sharper gradients and potentially greater HVAC cycling frequency.

Heat-flux analysis provided mechanistic insight into these observations. Low-conductivity, nano- or micro-porous materials suppressed early heat-transfer peaks and flattened flux curves, while fiber-aligned materials transferred heat more directly. Together with the time-constant analysis, this confirmed that microstructural topology including pore continuity, tortuosity, and channel alignment plays a decisive role in transient thermal moderation. A strong linear correlation ($\mathrm{R}^2 \approx 0.89$) was observed between intrinsic conductivity and cooling energy demand, enabling predictive estimation of material impact. The resulting empirical relation suggests that every 0.01 $\mathrm{W{\cdot}m^{-1}{\cdot}K^{-1}}$ conductivity reduction may yield approximately 1.1–1.4% energy savings under similar conditions. This provides a simple but powerful design tool for architects and engineers selecting interior finishes for energy-focused construction.

Overall, the findings demonstrate that interior finishing materials should be recognized not only as aesthetic elements but also as functional components of the building thermal system. Their role extends beyond steady-state insulation to active modulation of heat flow, energy consumption, and comfort stability. Adoption of nano-porous or fiber-based green finishes, particularly aerogel and cellulose composites, may support annual HVAC energy savings on the order of 7–15% in temperate climates. Further work

should examine long-term performance under humidity cycling, validate results in real buildings, and integrate finishing-layer parameters into building energy simulation frameworks. These outcomes point to an emerging design paradigm where finishing-layer engineering becomes a practical and scalable route toward low-carbon, high-comfort building interiors.

References

[1] International Energy Agency. (2022). *World Energy Outlook 2022*. Paris: IEA.
[2] Intergovernmental Panel on Climate Change. (2022). *Climate Change 2022: Mitigation of Climate Change*. Cambridge University Press.
[3] United Nations Environment Programme. (2023). *2023 Global Status Report for Buildings and Construction*. Nairobi: UNEP.
[4] Pérez-Lombard, L., Ortiz, J., and Pout, C. (2008). A review on buildings energy consumption information. *Energy and Buildings*, 40(3), 394–398.
[5] Santamouris, M. (2016). Innovating to zero the building sector in Europe. *Solar Energy*, 128, 61–94.
[6] Ascione, F., Bianco, N., De Masi, R. F., de'Rossi, F., and Vanoli, G. P. (2014). Energy refurbishment of existing buildings through the use of phase change materials: Energy savings and indoor comfort in the cooling season. *Applied Energy*, *113*, 990–1007.
[7] International Energy Agency. (2018). *The Future of Cooling*. Paris: IEA.
[8] U.S. Department of Energy. (2020). *Building Technologies Office Multi-Year Program Plan 2020–2030*. Washington, DC.
[9] European Commission. (2019). *Clean Energy for All Europeans Package*. Brussels.
[10] Khovalyg, D., Kazanci, O. B., Halvorsen, H., Gundlach, I., Bahnfleth, W. P., Toftum, J., and Olesen, B. W. (2020). Critical review of standards for indoor thermal environment and air quality. *Energy and Buildings*, 213, 109819.
[11] Medved, S. (2022). *Building Physics*. Springer.
[12] Janssen, H., and Van De Walle, W. (2022). The impact of pore structure parameters on the thermal conductivity of porous building blocks. *Construction and Building Materials*, *324*, 126681.
[13] Cahill, D. G., Braun, P. V., Chen, G., Clarke, D. R., Fan, S., Goodson, K. E., and Shi, L. (2014). Nanoscale thermal transport. II. 2003–2012. *Applied physics reviews*, *1*(1).

[14] Zhang, C., Xiao, F., and Wang, J. (2021). Design optimization of multi-functional building envelope for thermal insulation and exhaust air heat recovery in different climates. *Journal of Building Engineering*, *43*, 103151.

[15] Wang, X., Sun, X., and Yu, C. W. F. (2018). Building envelope with variable thermal performance. *Indoor and Built Environment*, 27(6), 729–733.

[16] Mavromatidis, L. E., Michel, P., El Mankibi, M., and Santamouris, M. (2010, December). Study on transient heat transfer through multilayer thermal insulation: Numerical analysis and experimental investigation. In *Building Simulation* (Vol. 3, No. 4, pp. 279–294). Heidelberg: Tsinghua Press.

[17] Nam, J., Choi, J. Y., Yuk, H., Kim, Y. U., Chang, S. J., and Kim, S. (2022). Thermal behavior analysis of wood-based furniture applied with phase change materials and finishing treatment for stable thermal energy storage. *Building and Environment*, *224*, 109534.

[18] Tunçbilek, E., Arıcı, M., Krajčík, M., Nižetić, S., and Karabay, H. (2020). Thermal performance based optimization of an office wall containing PCM under intermittent cooling operation. *Applied Thermal Engineering*, *179*, 115750.

[19] Anter, A. G., Sultan, A. A., Hegazi, A. A., and El Bouz, M. A. (2023). Thermal performance and energy saving using phase change materials (PCM) integrated in building walls. *Journal of Energy Storage*, *67*, 107568.

[20] Bourbia, S., Kazeoui, H., and Belarbi, R. (2023). A review on recent research on bio-based building materials and their applications. *Materials for Renewable and Sustainable Energy*, *12*(2), 117–139.

[21] Palani, H., Tang, M., Zhang, R., and Desjarlais, A. (2025). Assessing the hygrothermal performance of bio-based materials in building wall systems. *Construction and Building Materials*, *492*, 142907.

[22] Sathre, R., and O'Connor, J. (2010). Meta-analysis of greenhouse gas displacement factors of wood product substitution. *Environmental science & policy*, *13*(2), 104–114.

[23] Forte, A., Dourado, F., Mota, A., Neto, B., Gama, M., and Ferreira, E. C. (2021). Life cycle assessment of bacterial cellulose production. *The International Journal of Life Cycle Assessment*, *26*(5), 864–878.

[24] Koebel, M., Rigacci, A., and Achard, P. (2012). Aerogel-based thermal superinsulation: an overview. *Journal of sol-gel science and technology*, *63*(3), 315–339.

[25] Baetens, R., Jelle, B. P., and Gustavsen, A. (2011). Aerogel insulation for building applications: A state-of-the-art review. *Energy and buildings*, *43*(4), 761–769.

[26] Dorcheh, A. S., and Abbasi, M. H. (2008). Silica aerogel; synthesis, properties and characterization. *Journal of materials processing technology*, *199*(1–3), 10–26.

[27] Huang, X., Zhu, C., Lin, Y., and Fang, G. (2019). Thermal properties and applications of microencapsulated PCM for thermal energy storage: A review. *Applied Thermal Engineering*, *147*, 841–855.

[28] Cheng, Z., Xu, R., and Jiang, P. X. (2021). Morphology, flow and heat transfer in triply periodic minimal surface based porous structures. *International Journal of Heat and Mass Transfer*, *170*, 120902.

[29] Gibson, L. J., and Ashby, M. F. (1997). *Cellular solids: Structure and properties*. Cambridge University Press.

[30] Nicol, J. F., and Humphreys, M. A. (2002). Adaptive thermal comfort and sustainable thermal standards for buildings. *Energy and buildings*, *34*(6), 563–572.

[31] De Dear, R., Xiong, J., Kim, J., and Cao, B. (2020). A review of adaptive thermal comfort research since 1998. *Energy and Buildings*, *214*, 109893.

[32] Fanger, P. O. (1970). *Thermal comfort*. McGraw-Hill.

[33] Mendes, N., and Philippi, P. C. (2005). A method for predicting heat and moisture transfer through multilayered walls based on temperature and moisture content gradients. *International Journal of Heat and Mass Transfer*, *48*(1), 37–51.

[34] Khovalyg, D., Kazanci, O. B., Halvorsen, H., Gundlach, I., Bahnfleth, W. P., Toftum, J., and Olesen, B. W. (2020). Critical review of standards for indoor thermal environment and air quality. *Energy and Buildings*, *213*, 109819.

[35] Shen, Z., Brooks, A. L., He, Y., Shrestha, S. S., and Zhou, H. (2021). Evaluating dynamic thermal performance of building envelope components using small-scale calibrated hot box tests. *Energy and Buildings*, *251*, 111342.

Biography

Lu Peng graduated from the China Academy of Art and currently serves as a core faculty member, associate professor, and a key young faculty member in Hunan Province in the Architectural Decoration Construction Technology program at Hunan Urban Construction College. She has been a visiting scholar at Zhejiang University. Her research focuses on green decoration and smart home design. In recent years, she has led multiple national teaching guidance committee projects and provincial-level research initiatives. She has also overseen five third-phase supply-demand employment and education projects under the Ministry of Education. Under her guidance, students have won eight first and second prizes in national and provincial vocational college skills competitions. She has published multiple papers in journals such as *University* and *Decoration & Renovation*, authored four textbooks, published three monographs, and holds two invention patents.